CCFE
CULHAM CENTRE FOR FUSION ENERGY

UK Atomic Energy Authority

UKAEA-CCFE-CP(20)96

J. Simpson, D. Moulton, C. Giroud, D. Harting, G. Corrigan, M. Groth, JET Contributors

Upstream separatrix temperature dependence in EDGE2D-EIRENE for JET H-mode plasmas

Upstream separatrix temperature dependence in EDGE2D-EIRENE for JET H-mode plasmas

J. Simpson, D. Moulton, C. Giroud, D. Harting, G. Corrigan, M. Groth, JET Contributors

This paper has been submitted to
23rd International Conference on Plasma Surface Interactions in Controlled Fusion Devices (PSI), Princeton, NJ, USA, 17-22 June 2018

Using EDGE2D-EIRENE to simulate the effect of impurity seeding and fueling on the upstream electron separatrix temperature

J. Simpson[1,2], D. Moulton[1], C. Giroud[1], M. Groth[2], G. Corrigan[1] and JET Contributors*
[1] EUROfusion Consortium, JET, Abingdon, Oxfordshire, OX14 3DB, [2] Aalto University, 02150 Espoo
*See the author list of "X. Litaudon et al 2017 Nucl. Fusion 57 102001"

1 Abstract

The edge fluid code EDGE2D-EIRENE was used to study the effect of impurity seeding on the separatrix temperature. A comparison between the predicted upstream temperature from EDGE2D-EIRENE and the two point model upstream temperature equation was carried out. EDGE2D predicts a linear scaling between the upstream temperature ($T_{u,sep}$) and the power crossing the separatrix (P_{sep}); this is contrary to the scaling $T_{u,sep} \propto P_{sep}^{\frac{2}{7}}$, which is derived from the two point model assuming P_{sep} is the only significantly varying parameter. The scaling has not been observed in the EDGE2D-EIRENE simulations due to a factor six variation in parallel heat flux entering the divertor at the separatrix ($q_{\parallel,u,sep}$). The variation in $q_{\parallel,u,sep}$ is driven by factor two variation in P_{sep} and impurity radiation preferentially removing heat flux above the x-point and near the separatrix. This leads to a largely varying $q_{\parallel,u,sep}$ which is captured by the power decay length calculated by Eich fitting ($\lambda_{q,eich}$). Accounting for the $q_{\parallel,u,sep}$ variation, using $\lambda_{q,eich}$ and P_{sep}, an agreement between the two point model equation and the predicted upstream temperature from EDGE2D-EIRENE has been obtained. A variation of upstream electron temperature from 60 eV to 120 eV, for electron separatrix density range of $2 - 3 \times 10^{19}\ m^{-3}$, was observed. This separatrix temperature variation from EDGE2D is in contrast to a routinely assumed separatrix temperature of 100eV used for pedestal stability analysis at JET.

2 Introduction

The separatrix temperature is required as an input for several models of the tokamak edge. For example, the heuristic λ_q model in reference [1], H-mode density limit studies in reference [2] and pedestal stability analysis [3]. The separatrix temperature can be approximated by the two point model equation [4]:

$$T_{u,sep} = \left(\frac{7 q_{\parallel,u,sep} L}{2\kappa}\right)^{\frac{2}{7}}. \quad (1)$$

Here, $T_{u,sep}$ is the upstream electron/ion temperature (eV), which is assumed to be the low field side (LFS) midplane separatrix, $q_{\parallel,u,sep}$ is the electron/ion heat flux at the entrance to the divertor on the

LFS at the separatrix (Wm^{-2}), L is the connection length (m), and $\kappa = 60$ (W$m^{-1}eV^{-\frac{7}{2}}$), if considering the ion temperature, or $\kappa = 2000$ (W$m^{-1}eV^{-\frac{7}{2}}$) for the electron temperature.

Using the approximation $q_{\parallel,u,sep} \sim (P_{sep}/2)/A_q$ allows the derivation of an upstream temperature equation that contains directly-measured experimental variables [4]:

$$T_u = \left(\frac{2\ ((P_{sep}/2)/A_q)L}{7\ \kappa} \right)^{\frac{2}{7}}. \quad (2)$$

Here, P_{sep} is power crossing the last closed flux surface from the confined plasma (W) and,

$$A_q = 2\pi R \lambda_q \left(\frac{B}{B_\theta} \right), \quad (3)$$

Where A_q is the parallel area (m^2) that P_{sep} falls over, λ_q is the power decay width at the upstream position in (m), R is the radius at the upstream position, and $\left(\frac{B}{B_\theta}\right)$ is the ratio of the total magnetic field to poloidal magnetic field at the upstream location.

The upstream separatrix temperature has an impact on the pedestal stability. In reference [5] it was concluded that a decrease of ~20 eV in the separatrix temperature had a positive impact on pedestal stability. Neon seeding was not considered, which is known to radiate closer to and inside of the separatrix compared to nitrogen and thus could have a larger impact on the upstream separatrix temperature. Nitrogen seeding causes the pedestal height to increase, which has not been observed when seeding with neon [6]. The upstream temperature could be affected by impurity seeding which would in turn affect the pedestal structure. Work presented in references [7, 8] considered the effect of nitrogen seeding using EDGE2D-EIRENE. However, the authors focussed on the effect on the divertor and comparison to experiment rather than the upstream effects examined in this paper.

In this work the applicability of equation 2 has been assessed using the edge fluid neutral code EDGE2D-EIRENE [9, 10]. Simulations were conducted with varying neon and nitrogen seeding radiation and a range of electron separatrix densities ($n_{e,sep}$).

The scaling of the upstream temperature and power crossing the separatrix, i.e. $T_{u,sep} \propto P_{sep}^{\frac{2}{7}}$, can be derived from equation 1. This scaling assumes that all other parameters within equation 1 vary only by a small amount and have a weak power dependence. The fact that the power dependence of P_{sep} is so small further allows the assumption that the upstream temperature is essentially invariant. Using this assumption, a value of 100 eV is assumed for the JET upstream separatrix temperature, independent of specifics of a particular JET discharge. The 100 eV assumption is often made for pedestal stability analysis [5]. The legitimacy of the $T_{u,sep} \propto P_{sep}^{\frac{2}{7}}$ scaling will be assessed within this paper.

Impurities, either intrinsically sputtered or injected, deliberately introduce losses between the upstream and downstream locations. However, equation 2 assumes no energy losses between the upstream and x-point positions. Therefore, the validity of equation 2 due to this assumption has been examined in this work in order to provide guidance on its continued application.

3 Simulation set up

The edge fluid code EDGE2D, [9] coupled to the kinetic neutral Montel-Carlo code EIRENE [10] was used to simulate a high confinement mode plasma in a set up as shown in reference [11] (high field side (HFS) and LFS strike points located on vertical target). The main fuel puff location was the same as used in reference [11]. However the impurity puff location was moved to the LFS target in the private flux region so that it was in the same location as the experimental results presented in [6].

Simulations with two different seeding impurities – neon and nitrogen - were conducted. The impurities due to seeding were controlled within the simulation such that the total impurity seeding radiation achieved was either 2, 4 or 6 MW. For each seeded impurity and radiation, a scan in upstream $n_{e,sep}$ has been performed where the density was set to either $2, 2.5$ or $3 \times 10^{19}\ m^{-3}$. A total input power of 8 MW (split evenly between the ion and electron channel) was set as the core boundary condition for the heat flux into the domain. This parameter range was chosen to be representative of H-mode like conditions for seeding scenarios [6]. The $3 \times 10^{19}\ m^{-3}$, 6 MW, neon and nitrogen seeded simulations are not presented here due to code convergence issues. Unseeded reference cases were also simulated for each $n_{e,sep}$. Beryllium was also included as a sputtered impurity for the main chamber wall. Drifts were not included within these simulations.

The radial transport in EDGE2D-EIRENE is diffusive only and prescribed. The radial particle and heat diffusion profiles were taken directly from [11, 12] for the main ions and electrons, and remained fixed throughout the presented parameter scan. Below the x-point the radial particle transport coefficients were set to $1\ m^2 s^{-1}$ for the main ion and electrons. For the impurity ions it was assumed that the radial particle transport is poloidally and radially constant at $0.6\ m^2 s^{-1}$ both above and below the x-point. The choice of the impurity transport coefficient is arbitrary, yet reasonable, due to having limited experimental knowledge about the radial transport of the impurity ions and this aided in code convergence. The inclusion of a particle transport barrier in the radiating impurity was tested because a transport barrier was used in the main ions. At low upstream separatrix density, the upstream electron temperature increased up to approximately 40%. However, the impurity transport barrier was found to produce very large core $Z_{effective}$ values, which were not experimentally relevant. At the highest electron separatrix density within this parameter scan, the transport barrier had minimal effect on the upstream temperature and $Z_{effective}$.

4 Results

The purpose of this study was to compare the predicted upstream temperature from EDGE2D-EIRENE with the prediction by equation 2. EDGE2D-EIRENE was used as a synthetic experiment; parameters P_{sep}, L and A_q were extracted from EDGE2D to calculate equation 2 for comparison with the upstream temperature predicted by EDGE2D.

4.1 Scaling of the upstream temperature with $q_{\parallel}$ and P_{sep}

The derivation of equation 1 is based on the following assumptions: (1) the heat transport from the upstream to the downstream location is exclusively conductive and calculated according to Spitzer-Härm [4]; (2) T_u is much greater than downstream temperature i.e. $T_u^{\frac{2}{7}} \gg T_t^{\frac{2}{7}}$; (3) κ remains constant along a field line and; (4) $Lq_{\parallel,u}$ captures the entire variation of the heat flux along the field line, i.e. $\int_0^{L_u} q_{u,\parallel} ds_\parallel \sim L_u q_{u,\parallel}$.

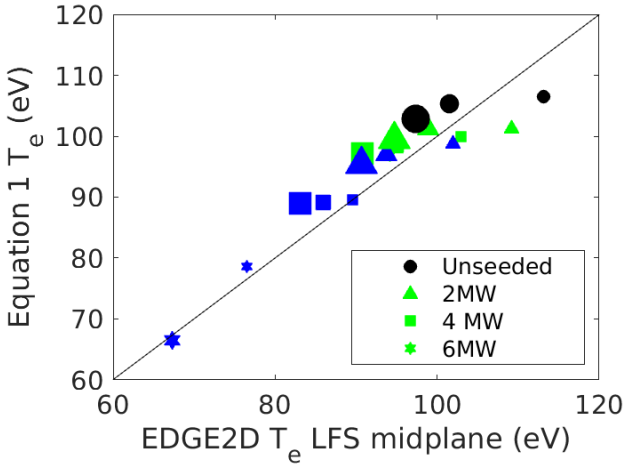

Figure 1 – The upstream electron temperature calculated using the two point model equation $T_{u,sep} = \left(\frac{7q_\parallel L}{2\kappa}\right)^{\frac{2}{7}}$ plotted against the EDGE2D temperature taken at the LFS midplane. The markers represent the total seeding radiation: circle – 0MW (i.e. unseeded); triangle – 2MW; square – 4MW; 6-point star – 6MW. The colour represents the seeding impurity: black – unseeded; green – nitrogen; blue – neon. Increasing size of the symbol represents increasing electron separatrix density ($n_{e,sep}$) where the smallest symbol is $n_{e,sep} = 2 \times 10^{19}$and the largest is $n_{e,sep} = 3 \times 10^{19}$.

First, it must be established whether the assumptions stated in the previous paragraph can be validated within the presented parameter scan in order to proceed with a comparison of equation 2. Equation 1 was calculated using $q_\parallel$ at the divertor entrance at the separatrix ($q_{\parallel,u,sep}$). L is calculated to the LFS midplane for all cases, and $\kappa = 2000$. Figure 1 shows an agreement between the upstream electron separatrix temperature measured in EDGE2D-EIRENE and the prediction from equation 1. Note the low density unseeded case (smallest black circle) is sheath limited, and when including the target temperature in equation 1 this gives a better agreement with EDGE2D. The agreement was approximately within 20 % at worst, and so a comparison with equation 2 was carried out.

The scaling $T_u \propto q_{\parallel,u,sep}^{\frac{2}{7}}$ can be derived from equation 1. For this simulation set, the scaling is valid due to all other variables in equation 1 (except $q_{\parallel,u,sep}$) being constant because the equilibrium remained fixed throughout the simulation set. Using this scaling, roughly a factor six change in $q_{\parallel,u,sep}$ at the divertor entrance has been observed (figure 2); hence the large variation in $q_{\parallel,u,sep}$ drives the two fold variation in $T_{u,sep}$.

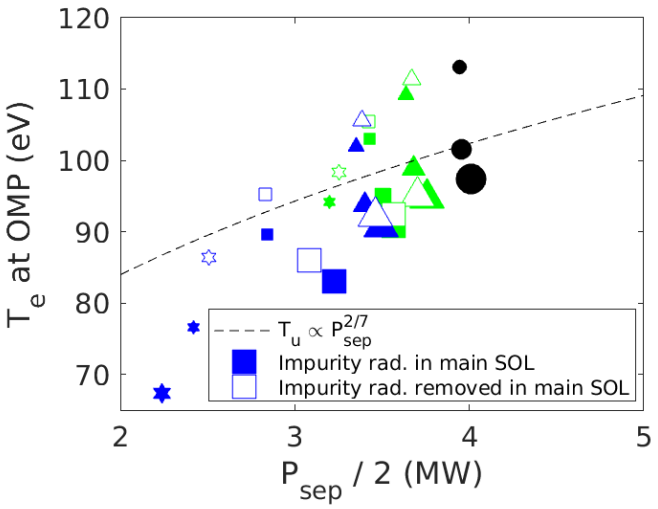

Figure 2 - Upstream (outer midplane) temperature versus power crossing the separatrix divided by 2 (assuming 50% split to HFS and LFS targets). The markers represent the total seeding radiation: circle – 0 MW (i.e. unseeded); triangle – 2 MW; square – 4 MW; 6-point star – 6 MW. The colour represents the seeding impurity: black – unseeded; green – nitrogen; blue – neon. Increasing size of the symbol represents increasing electron separatrix density ($n_{e,sep}$) where the smallest symbol is $n_{e,sep} = 2 \times 10^{19}$and the largest is $n_{e,sep} = 3 \times 10^{19}$. The open symbols represent the same plasma parameters as the filled markers except within the simulation the impurity radiation has been removed from the scrape-off layer above the x-point. The dotted line represents $T_u = AP_{sep}^{\frac{2}{7}}$ where A was chosen to roughly fit the data.

Equation 2 can be approximated by $T_{u,sep} \propto P_{sep}^{\frac{2}{7}}$. Based on the observation that $T_{u,sep} \propto q_{\parallel,u,sep}^{\frac{2}{7}}$ scaling is correct and $q_{\parallel,u,sep}$ varies by a factor six, it could be expected that P_{sep} would also vary by a factor six. However, a linear scaling between $T_{u,sep}$ and P_{sep} was found (figure 2 solid markers), thus P_{sep} only varies by roughly a factor two which would not support a factor six variation in upstream temperature. Hence, for the presented simulations, equation 2 cannot be simplified to $T_{u,sep} \propto P_{sep}^{\frac{2}{7}}$ and does not fully explain the factor two variation in $T_{u,sep}$.

4.2 Variation in P_{sep} is driven by core impurity radiation

A one-to-one correlation (within 1%) between the input power (into the grid) minus core impurity radiation and P_{sep} was observed (figure 3). This implies that the observed variation in P_{sep} is dictated by the amount of impurity radiation occurring inside the separatrix.

Comparing the radiative loss function [4] for a neon and nitrogen [13] case with identical $n_{e,sep}$ and total impurity radiation, it was found that neon radiates more efficiently inside the separatrix than nitrogen [13]. Hence in all cases where $n_{e,sep}$ and total impurity radiation was the same, neon has a lower P_{sep} than nitrogen.

The variation in P_{sep} was only a factor and two (figure 2) and does not fully explain the observed the $T_{u,sep}$ variation.

4.3 Additional variation $q_{\parallel,sep}$ is driven by main SOL impurity radiation above the x-point

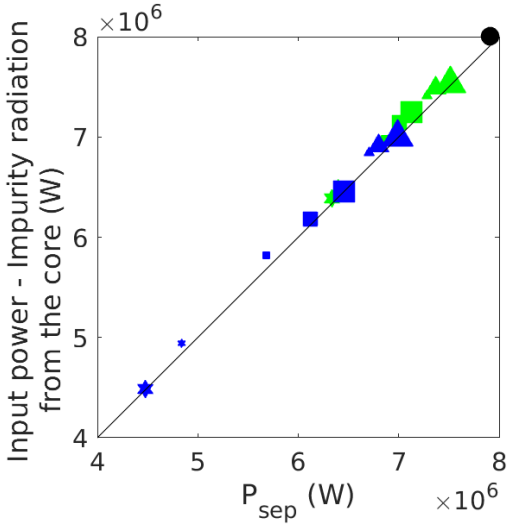

Figure 3 - Input power (always 8 MW) to the computational domain minus the total impurity radiation within the separatrix versus the power crossing the separatrix. The markers represent the total seeding radiation: circle – 0 MW (i.e. unseeded); triangle – 2 MW; square – 4 MW; 6-point star – 6 MW. The colour represents the seeding impurity: black – unseeded; green – nitrogen; blue – neon. Increasing size of the symbol represents increasing electron separatrix density ($n_{e,sep}$) where the smallest symbol is $n_{e,sep} = 2 \times 10^{19}$and the largest is $n_{e,sep} = 3 \times 10^{19}$.

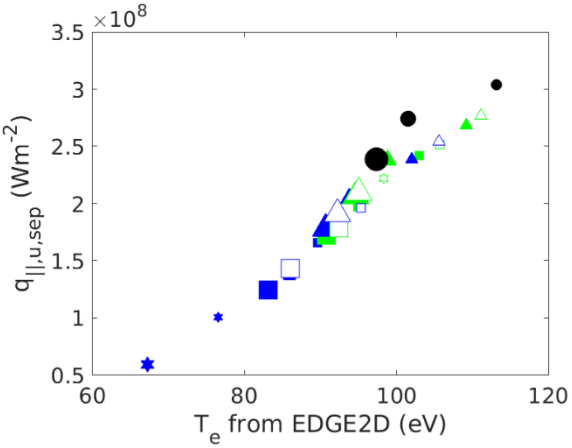

Figure 4 - The upstream electron separatrix temperature from EDGE2D plotted against the parallel heat flux at the separatrix at the divertor entrance. The markers represent the total seeding radiation: circle – 0 MW (i.e. unseeded); triangle – 2 MW; square – 4 MW; 6-point star – 6 MW. The colour represents the seeding impurity: black – unseeded; green – nitrogen; blue – neon. Increasing size of the symbol represents increasing electron separatrix density ($n_{e,sep}$) where the smallest symbol is $n_{e,sep} = 2 \times 10^{19}$and the largest is $n_{e,sep} = 3 \times 10^{19}$ The open symbols represent the same plasma parameters as the filled symbols except within the simulation the impurity radiation has been removed from the scrape-off layer above the x-point.

A reduction in $q_{\parallel,u,sep}$ was observed when the impurity radiation was present (figure 4). For a fixed $n_{e,sep}$ an increase in the total impurity radiation leads to a reduction in $q_{\parallel,u,sep}$ (figure 4). Furthermore, for a comparable simulation, similar $n_{e,sep}$ and total impurity radiation, neon seeding causes a larger reduction in $q_{\parallel,sep}$ than nitrogen compared to an unseeded case (figure 4).

To confirm that impurity radiation was the main mechanism for the variation in the $q_{\parallel,sep}$, a code study has been conducted. The code study removes the impurity radiation from the main SOL (above the x-point) only, but still allows for impurity radiation in the divertor (below x-point) and core (inside separatrix) hence keeping P_{sep} roughly the same. The goal of this study was to assess the effect on the $q_{\parallel,sep}$ at the LFS divertor entrance when impurity radiation was removed in the main SOL. The impurity radiation was set to 2, 4 or 6 MW depending on the simulation chosen minus the contribution of the impurity radiation in the main SOL of that simulation. The reason for setting the radiation in this manner was to ensure the same impurity radiation in the core and divertor regions when seeding radiation was present in the main SOL. The study was run for seeding cases which had an $n_{e,sep}$ of 2×10^{19} and $3 \times 10^{19}\ m^{-3}$.

The code study simulations showed a decreased variation in $q_{\parallel,u,sep}$ at the divertor entrance (figure 4, open symbols). Therefore, the electron $T_{u,sep}$ variation, in the code study, is observed to reduce by 15% (open symbols figure 4). The code experiment shows that the impurity radiation is in part responsible for the $q_{\parallel,u,sep}$ variation.

The code study simulations follow the $T_u \propto P_{sep}^{\frac{2}{7}}$ (where T_u was taken as the electron separatrix temperature from EDGE2D) scaling because P_{sep} is now the main driver of the $q_{\parallel,u,sep}$ at the divertor entrance (open symbols figure 2). However, there is still some variation $q_{\parallel,u,sep}$ due to other simulation parameters and hence the code do not follow exactly the plotted $T_u \propto P_{sep}^{\frac{2}{7}}$ line. What is important is that the scaling ($T_u \propto P_{sep}^{\frac{2}{7}}$) is almost recovered and that it is no longer linear (open symbols figure 2).

4.4 Variation in λ_q captures the variation in $q_{\parallel,sep}$

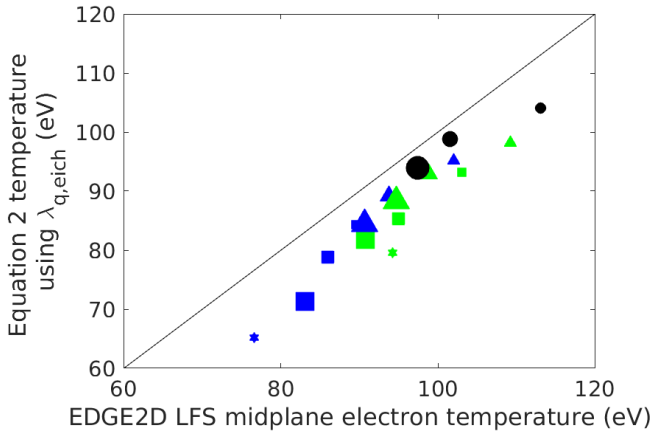

Figure 5 - The upstream temperature from EDGE2D-EIRENE compared to the two point model equation [4]. The two point model equation is calculated using the power decay width (λ_q) from the Eich fit. The markers represent the total seeding radiation: circle – 0 MW; triangle – 2 MW; square – 4 MW; 6-point star – 6 MW. The colour represents the seeding impurity: black – unseeded; green – nitrogen; blue – neon. Increasing size of the symbol represents increasing electron separatrix density ($n_{e,sep}$) where the smallest symbol is $n_{e,sep} = 2 \times 10^{19}$and the largest is $n_{e,sep} = 3 \times 10^{19}$.

The total $q_{\parallel}$ profile of the outer target was fitted using the Eich fit [14] to calculate $\lambda_{q,eich}$ for each simulation. Using $\lambda_{q,eich}$ a value for A_q has been calculated (as per equation 3) which from now onwards will be referred to as $A_{q,eich}$. Extracting P_{sep}, L and B_θ/B (note L and B_θ/B are constant throughout the whole simulation set as the same equilibrium was used) from EDGE2D and using $A_{q,eich}$, an upstream temperature has been calculated using equation 2. A comparison between this recalculated upstream temperature and the upstream temperature from EDGE2D is shown in figure 5. Agreement within approximately 20% of the predicted EDGE2D-EIRENE upstream temperature and the upstream temperature calculated from equation 2 has been found (figure 5). Note that there is, at worst, a systematic underprediction of approximately 20% (figure 5) of the upstream temperature calculated from equation 2 when compared EDGE2D. Accounting for the variation in both $\lambda_{q,eich}$ and P_{sep} in each simulation, agreement between equation 2 and EDGE2D was yielded.

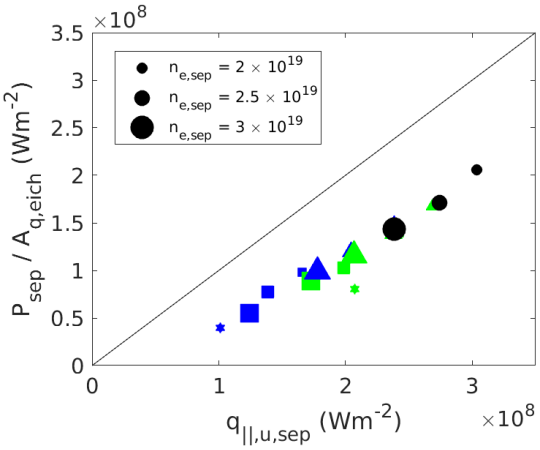

Figure 6 - $q_{\parallel,u,sep}$ plotted against the power crossing the separatrix (P_{sep}) divided by the area ($A_{q,eich}$) which is calculated using equation 3 and λ_q is taken as value calculated by the Eich fit. The markers represent the total seeding radiation: circle – 0 MW; triangle – 2 MW; square – 4 MW; 6-point star – 6 MW. The colour represents the seeding impurity: black – unseeded; green – nitrogen; blue – neon. Increasing size of the symbol represents increasing electron separatrix density ($n_{e,sep}$) where the smallest symbol is $n_{e,sep} = 2 \times 10^{19}$and the largest is $n_{e,sep} = 3 \times 10^{19}$

Equation 2 agrees with EDGE2D (figure 5) because $(P_{sep}/2)/A_{q,eich}$ captures the variation in $q_{\parallel,u,sep}$ (figure 6). This validates the assumption that $q_{\parallel,u,sep} \sim (P_{sep}/2)/A_q$ and hence why equation 2 agrees with EDGE2D. There is a large variation in $A_{q,eich}$ as $\lambda_{q,eich}$ varies by a factor four over the simulation set (horizontal lines figure 7). The variation of both P_{sep} and $A_{q,eich}$ explains the variation in T_u in experimentally measurable variables.

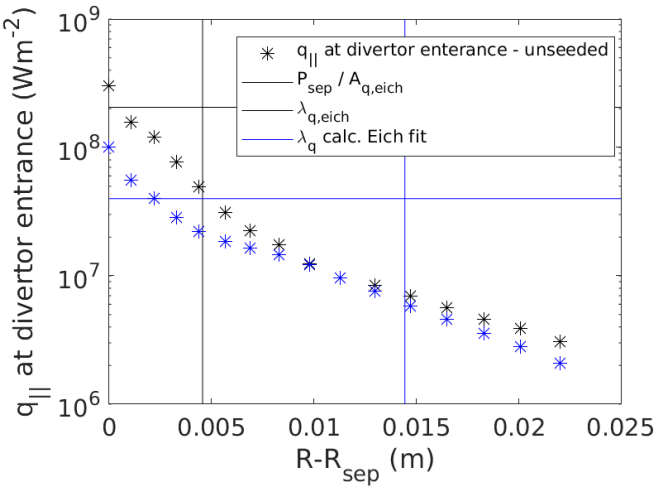

Figure 7 –Log plot of the parallel heat flux profle ($q_\parallel$) entering the divertor plotted against LFS midplane coordinate. Black markers represent the $q_\parallel$ for an unseeded $n_{e,sep} = 2 \times 10^{19}$ and blue markers the neon seeded $n_{e,sep} = 2 \times 10^{19}$. Horizontal lines represent P_{sep}/A_q where P_{sep} is the power crossing the separatrix and A_q is calculated as per equation 3 using λ_q calculated from the Eich fit and the colour retains the same meaning as the marker. Solid horizontal lines are λ_q calculated via the Eich fit and the colour retains the same meaning.

The Eich is used to calculate λ_q because it correctly captures the variation in $q_{\parallel,sep}$. The radial variation in the $q_\parallel$ profile at the divertor entrance has changed from a typical exponential decay from the separatrix to far SOL (unseeded case - black markers figure 7) to an exponential decay that has been clipped off near the separatrix (seeded case - blue markers figure 7), but retains the exponential decay shape in the far SOL. The reason why the exponential is clipped off is due to the preferential removal of power caused by the impurity radiation above the x-point. This change in the radial variation of the $q_\parallel$ profile (and $q_{\parallel,sep}$) to a non-exponential decay was captured well by the Eich fit. This non-exponential decay can be seen on figure 7 (blue markers) for around $R - R_{omp} = 0.002 - 0.01\ m$. Furthermore, the Eich fit is experimentally measurable, compared to measuring λ_q at the divertor entrance, which experimentally can be difficult.

5 Conclusion

A two-fold increase in upstream temperature has been observed within EDGE2D, which is driven by a factor six change in the parallel heat flux entering the divertor at the separatrix ($q_{\parallel,u,sep}$) thus confirming the scaling $T_u \propto q_{\parallel,u,sep}^{\frac{2}{7}}$. However, only a factor two change in the power crossing the separatrix (P_{sep}) was observed. P_{sep} (for constant input power) is exclusively set by the impurity radiation occurring on closed field lines. P_{sep} was lower for neon seeded cases to a comparable nitrogen seeded case because neon radiates more efficiently in the core than nitrogen, hence reducing P_{sep} and thus $T_{u,sep}$. Variation in $A_{q,eich}$ was driven by the clipping of the near SOL $q_\parallel$ profile at the divertor entrance, which renders the profile non-exponential. Nevertheless, our work shows that the Eich fit (which was used to calculate $A_{q,eich}$) can still be used in conjunction with P_{sep} to approximate $q_{\parallel,u,sep}$.

Once the variation of $q_{\parallel,usep}$ was accounted for (by using experimentally derived variables P_{sep} and $\lambda_{q,eich}$) an agreement within 20 % between EDGE2D-EIRENE upstream temperature and the two point model equation (equation 2) was yielded. A variation of upstream electron temperature from 60 to 120 eV with seeding, for $n_{e,sep}$ range of $2 - 3x10^{19}\ m^{-3}$, was observed. Hence it is incorrect to assume that the separatrix temperature is invariant due to the weak power scaling shown above. Models that are sensitive to the separatrix temperature should calculate λ_q and P_{sep} to predict an upstream temperature using the two point model equation.

6 References

[1] R.J. Goldston, Heuristic drift-based model of the power scrape-off width in low-gas-puff H-mode tokamaks, Nucl. Fusion. 52 (2012) 013009. doi:10.1088/0029-5515/52/1/013009.

[2] T. Eich, Correlation of the tokamak H-Mode density limit with ballooning stability at the separatrix, Nucl. Fusion. 58 (2018) 034001. doi:https://doi.org/10.1088/1478-3975/aa9768.

[3] H.R. Wilson, P.B. Snyder, G.T. A. Huysmans, R.L. Miller, Numerical studies of edge localized instabilities in tokamaks, Phys. Plasmas. 9 (2002) 1277. doi:10.1063/1.1459058.

[4] P. C. Stangeby, The Plasma Boundary of Magnetic Fusion Devices, 2000.

[5] S. Saarelma, A. Järvinen, M. Beurskens, C. Challis, L. Frassinetti, C. Giroud, M. Groth, M. Leyland, C. Maggi, J. Simpson, The effects of impurities and core pressure on pedestal stability in Joint European Torus (JET), Phys. Plasmas. 22 (2015). doi:10.1063/1.4921413.

[6] C. Giroud, G.P. Maddison, S. Jachmich, F. Rimini, M.N.A. Beurskens, I. Balboa, S. Brezinsek, R. Coelho, J.W. Coenen, L. Frassinetti, E. Joffrin, M. Oberkofler, M. Lehnen, Y. Liu, S. Marsen, K. McCormick, A. Meigs, R. Neu, B. Sieglin, G. Van Rooij, G. Arnoux, P. Belo, M. Brix, M. Clever, I. Coffey, S. Devaux, D. Douai, T. Eich, J. Flanagan, S. Grünhagen, A. Huber, M. Kempenaars, U. Kruezi, K. Lawson, P. Lomas, C. Lowry, I. Nunes, A. Sirinnelli, A.C.C. Sips, M. Stamp, S. Wiesen, Impact of nitrogen seeding on confinement and power load control of a high-triangularity JET ELMy H-mode plasma with a metal wall, Nucl. Fusion. 53 (2013). doi:10.1088/0029-5515/53/11/113025.

[7] A.E. Jaervinen, M. Groth, M. Airila, P. Belo, M. Beurskens, S. Brezinsek, M. Clever, G. Corrigan, S. Devaux, P. Drewelow, T. Eich, C. Giroud, D. Harting, A. Huber, S. Jachmich, K. Lawson, B. Lipschultz, G. Maddison, C. Maggi, T. Makkonen, C. Marchetto, S. Marsen, G.F. Matthews, A.G. Meigs, D. Moulton, M.F. Stamp, S. Wiesen, M. Wischmeier, Interpretation of radiative divertor studies with impurity seeding in type-I ELMy H-mode plasmas in JET-ILW using EDGE2D-EIRENE, J. Nucl. Mater. 463 (2015) 135–142. doi:10.1016/j.jnucmat.2014.10.047.

[8] A.E. Jaervinen, S. Brezinsek, C. Giroud, M. Groth, C. Guillemaut, P. Belo, M. Brix, G. Corrigan, P. Drewelow, D. Harting, A. Huber, K.D. Lawson, B. Lipschultz, C.F. Maggi, G.F. Matthews, A.G. Meigs, D. Moulton, M.F. Stamp, S. Wiesen, Impact of divertor geometry on radiative divertor performance in JET H-mode plasmas, Plasma Phys. Control. Fusion. 58 (2016) 45011. doi:10.1088/0741-3335/58/4/045011.

[9] S. Wiesen, ITC Report, www.eirene.de/e2deir_ report_30jun06.pdf, 2006.

[10] D. Reiter, C. May, D. Coster, R. Schneider, Time dependent neutral gas transport in tokamak edge plasmas, J. Nucl. Mater. 220–222 (1995) 987–992. doi:10.1016/0022-3115(94)00648-2.

[11] A.E. Jaervinen, M. Groth, M. Airila, P. Belo, M. Beurskens, S. Brezinsek, M. Clever, G. Corrigan, S. Devaux, P. Drewelow, T. Eich, C. Giroud, D. Harting, A. Huber, S. Jachmich, K. Lawson, B. Lipschultz, G. Maddison, C. Maggi, T. Makkonen, C. Marchetto, S. Marsen, G.F. Matthews, A.G. Meigs, D. Moulton, M.F. Stamp, S. Wiesen, M. Wischmeier, Interpretation of radiative divertor studies with impurity seeding in type-I ELMy H-mode plasmas in JET-ILW using EDGE2D-EIRENE, J. Nucl. Mater. 463 (2015) 135–142. doi:10.1016/j.jnucmat.2014.10.047.

[12] D.J. Moulton, Numerical Modelling of H-mode Plasmas on JET, PhD Theisis, (2012).

[13] A. Järvinen, Radiative divertor studies in JET high confinement mode plasmas, PhD Theisis, 2015. https://aaltodoc.aalto.fi/handle/123456789/18491.

[14] T. Eich, B. Sieglin, A. Scarabosio, W. Fundamenski, R.J. Goldston, A. Herrmann, Inter-ELM power decay length for JET and ASDEX Upgrade: Measurement and comparison with heuristic drift-based model, Phys. Rev. Lett. 107 (2011) 1–4. doi:10.1103/PhysRevLett.107.215001.